JOURNAL OF X-RAY SCIENCE AND TECHNOLOGY 4, 8–17 (1993)

Characterization of a Flat-Field Grazing-Incidence XUV Spectrometer

W. SCHWANDA,* K. EIDMANN,* AND M. C. RICHARDSON†

*Max-Planck-Institut für Quantenoptik, 85740 Garching, Germany; and †Center for Research in Electro-Optics and Lasers, 12424 Research Parkway, Orlando, Florida 32892

Received September 29, 1992

We describe a XUV spectrometer for the study of dense hot microplasmas at wavelengths between ≈50 and ≈300 Å. It uses a commercially fabricated grazing incidence flat-field reflection grating with 1200 grooves per millimeter. The spectral resolution was optimized by imaging the source on a narrow slit with the help of a curved grazing incidence mirror. The instrument was tested with a laser-produced plasma as a source. The limit of the resolving power due to imaging aberrations of the flat-field grating ranges from 1500 at 50 Å to 3600 at 200 Å and has been achieved with a 5-μm slit. We also measured and calculated the grating efficiencies for the first to fifth diffraction order as a function of wavelength. © 1993 Academic Press, Inc.

INTRODUCTION

The x-ray emission from hot dense microplasmas such as laser-produced plasmas is important for basic spectroscopic studies as well as for various applications, for example in the field of inertial confinement fusion or soft x-ray lasers. A large fraction of radiation is emitted by this type of plasma in the sub-keV photon energy region. Spectrometers for this range use either transmission gratings (*1, 2*) or reflection gratings under grazing incidence (*3*). Recently reflection gratings with nonequally spaced grooves have been developed for a so-called flat-field spectrometer (FFS) with the advantage of focusing the spectrum on a flat plane instead of on the curved Rowland circle (*4–6*). With such an instrument an extreme high resolving power of 35,000 has been achieved recently (*6*).

For the purpose of studying the emission from laser-produced plasmas we have built a FFS with a mechanically ruled flat-field grating (FFG) with 1200 grooves per millimeter fabricated by Hitachi, Ltd. (*7*). FFSs described previously use either no entrance slit (*8*) or an entrance slit at some distance to the source (*5, 9*). In the first case the spectral resolution is limited by the source size, whereas in the latter case only a small amount of light is collected by the slit. Also the slit may be damaged by the plasma blow-off, if positioned too close to the source. To avoid these drawbacks we image the source onto the entrance slit with the help of a curved grazing incidence mirror. In this way we use efficiently the radiation energy emitted by the source, which allows us to use narrow entrance slits in order to optimize the spectral resolution. In addition the short wavelength reflectivity cutoff of the grazing incidence mirror helps

0895-3996/93 $5.00

to suppress higher diffraction orders, which have large efficiencies, especially for short wavelengths as shown below.

In the following we characterize our FFS setup, which was tested with a laser-produced plasma as a soft x-ray source. We measured the spectral resolution with both x-ray film and an x-ray streak camera as a detector. Also values for the grating efficiencies in first and higher diffraction orders will be given.

SETUP

The experimental setup of the FFS is shown schematically in Fig. 1. The source is a laser plasma, which is generated by focusing a frequency doubled Nd-laser onto a flat solid target. The laser delivers energies up to 15 J within 3 ns (FWHM). The size of the x-ray source was 100 to 300 μm in diameter depending on the focusing of the laser beam. A spherical concave gold mirror is used under grazing incidence to image the source into the plane of the slit, which then is imaged by the FFG into the detector plane. Because of the grazing incidence, both the spherical collector mirror and the FFG act as cylindrical lenses and focus the light only in one direction (perpendicular to the plane of Fig. 1). The diameter of the spherical collector mirror was 50 mm, its radius of curvature 7 m, and the graze angle of incidence 2.2°. The mirror was positioned at a distance of 269 mm from both the source and the slit. The acceptance angle of the spherical mirror and of the FFG are matched to each other, and thus the whole surface of the FFG is illuminated. The collecting mirror was of standard optical quality. The disadvantage of having scattering losses in the imaging was tolerated in favor of considerably lower costs compared to the use of a high quality x-ray mirror.

The employed FFG is described in detail in Refs. (5, 7). It has a varying line spacing from 1095 to 1450 grooves per millimeter and works at a graze angle of incidence of

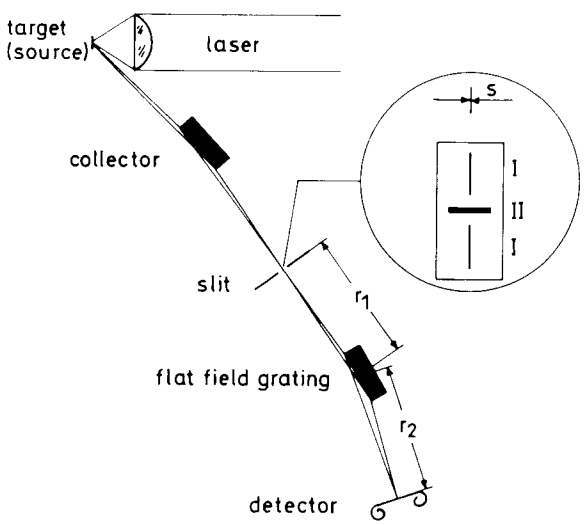

FIG. 1. Scheme of the flat-field spectrometer setup. The distances r_1 and r_2 are 237 and 235 mm, respectively. The used slit combination is shown separately on a magnified scale.

3°. It is blazed at an angle of 3.2° and designed for the wavelength range 50 to 300 Å. The substrate has a concave spherical surface with a radius of curvature of 5649 mm. It has a rectangular shape with a size of 30 mm along the grooves and 50 mm across the grooves.

As detectors we used either Kodak 101-01 x-ray film for time-integrated spectra or an x-ray streak camera (XRSC) with an CsI-cathode[10] for time-resolved spectra. The FFS has been operated in a vacuum chamber at pressures 10^{-2} to 10^{-5} Torr without taking special care of clean vacuum conditions (the target chamber is opened frequently in this type of laser-plasma experiment).

A special slit combination has been used, which is shown magnified in Fig. 1. It has at the top and the bottom a narrow slit (labeled I) and in the middle an aperture of $\approx$5 mm width and of small hight (labeled II). Thus one simultaneously obtains spectra that are source-size-limited and spectra that are of slit-limited-resolution, as shown in Fig. 2. The purpose of this slit combination is to facilitate the alignment: the slit is shifted laterally until the lines (and the zeroth order) are centered to each other. Under this condition the slit-limited spectrum stems from the central part of the source.

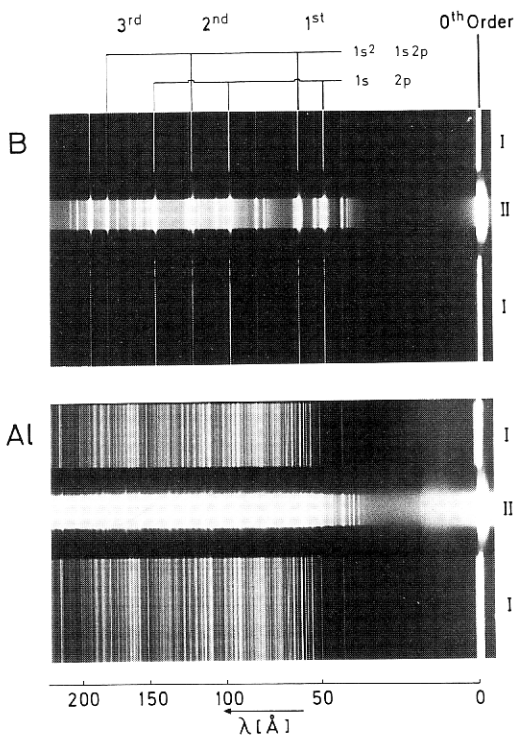

FIG. 2. Time-integrated spectra of boron and aluminum on Kodak 101-01 x-ray film. Laserenergy: 10J for B and 2J for Al, spot size 100 μm. The spectra at I (slit limited resolution) and II (source size limited resolution) stem from the corresponding slits as indicated in Fig. 1.

As target material we used boron and aluminum for the spectra in Fig. 2. The most intense lines in the boron spectrum are the transitions $1s^2 - 1s2p$ of B^{3+} and $1s - 2p$ of B^{4+}, which appear in first, second, and third order. A densitometer trace of the more complicated aluminum spectrum is shown in Fig. 3. It consists mainly of lines of Al^{9+} and Al^{10+} in different diffraction orders. Three particular lines having a fine structure are plotted separately in Fig. 3 on a magnified wavelength scale. They have been measured with different slit widths in order to demonstrate the influence of the slit width on resolution. The improvement in resolution when reducing the slit width from 20 to 5 μm is clearly seen.

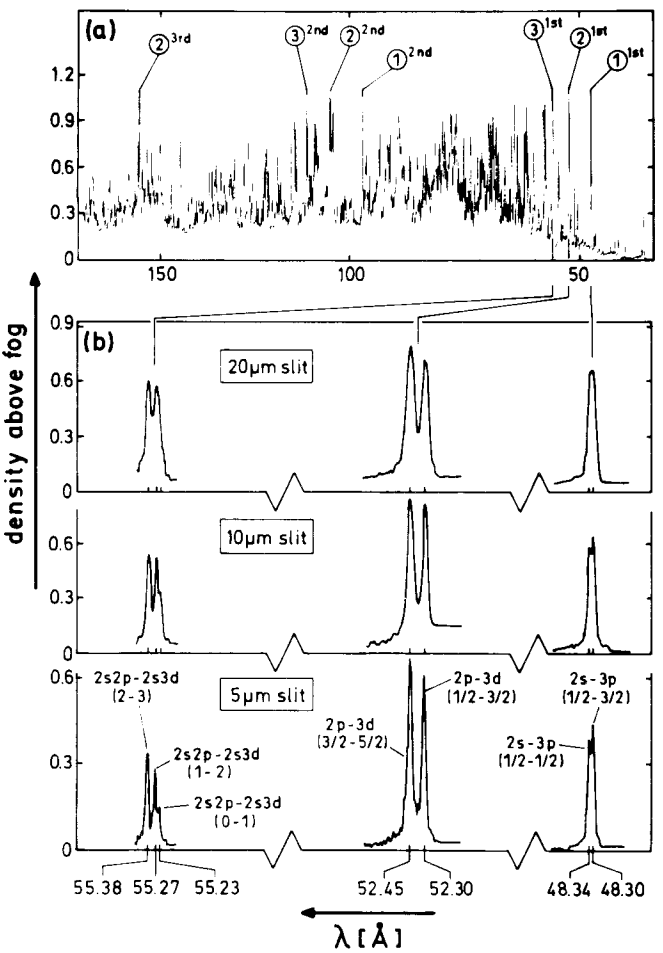

FIG. 3. (a) Densitometer trace of an aluminum spectrum: (b) resolution achieved with different slit widths demonstrated for three lines having fine-structure: $1s^22s2p - 1s^22s3d(Al^{9+})$, $1s^22p - 1s^23d(Al^{10+})$ and $1s^22s - 1s^23p(Al^{10+})$ (the numbers in brackets given in the figure denote the quantum number J of total angular momentum of the different multiplet components).

An example of an aluminum spectrum recorded by the XRSC is presented in Fig. 4. The lines labeled with the numbers 1, 2, and 3 are identical to those in the aluminum spectrum in Fig. 3. Due to the reduced spectral resolution achievable with the XRSC, the fine structure is no more resolved.

As a benefit from the collector mirror only a few joules of laser energy were necessary to measure the spectra presented in Figs. 2 to 4.

SPECTRAL RESOLUTION

The diffraction limit for the resolving power in first diffraction order is given by $\lambda/\Delta\lambda = N$, where N is the number of grooves, which is $\approx$60,000 for the present FFG. However, this optimum value is not attainable because of practical limitations such as imaging aberrations of the FFG or finite spatial resolution of the detector. In Fig. 5 we summarize the instrumental wavelength resolution $\Delta\lambda$ achieved with the present FFS under different conditions. $\Delta\lambda$ is defined as the halfwidth (FWHM) of a sufficiently narrow line (to ensure that the source determined Doppler and Stark line-broadening is small compared to the instrumental broadening we only employed those lines, whose width did not increase in higher orders). Lines in the range 50 to 60 Å have been employed for the data in Fig. 5. The distances r_1 and r_2 had been optimized for optimum resolution and were within ± 1 mm identical with the specified values (5)

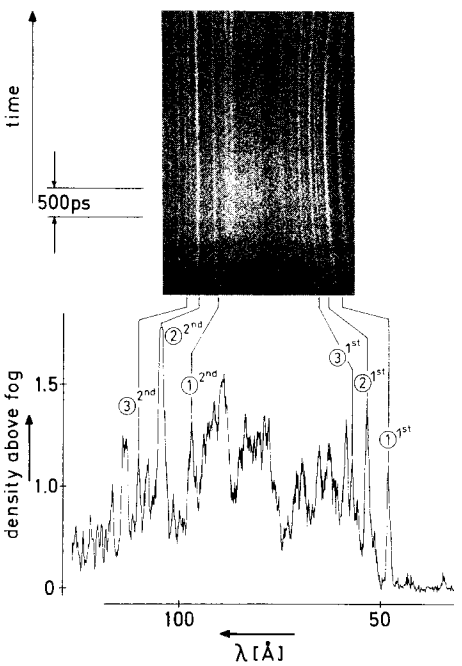

FIG. 4. Top: Al-spectrum measured with an x-ray streak camera (recorded on T-max film coupled to the output of the streak camera). Laser energy 2J, slit width 20 μm. Bottom: densitometer trace at a fixed time; the encircled numbers correspond to those in Fig. 3.

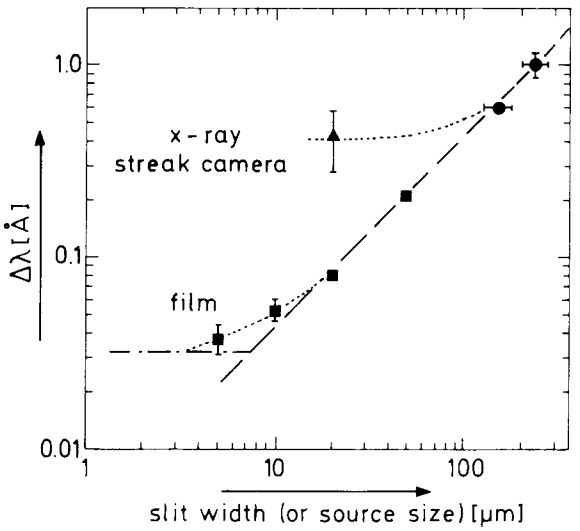

FIG. 5. Spectral wavelength resolution $\Delta\lambda$ for different conditions (see text).

(given in Fig. 1). The best values for $\Delta\lambda$ were obtained with Kodak 101-01 film as a detector and with small slit widths (squares in Fig. 5). In addition Fig. 5 shows the source size limited values for $\Delta\lambda$ (full dots, the optical spot size was taken as source size as the value for the abscissa) and a value obtained with the XRSC and a 20-μm slit.

The dashed straight line represents the wavelength resolution $\Delta\lambda$ resulting from the finite slit width s, which is imaged (with magnification 1) onto the detector plane. It follows the relation $\Delta\lambda = (d\lambda/dx)s$, where $d\lambda/dx$ is the inverse linear dispersion ($d\lambda/dx = 4.3$ Å/mm at 50 Å). Because of its finite spatial resolution of ≈ 100 μm [see Ref. (*10*)] the XRSC yields a wavelength resolution $\Delta\lambda$ which cannot be improved for slitwidths ≤ 100 μm. On the other hand, spatial resolution is not a limiting factor for the 101 film, which according to the measurements of Henke *et al.* (*11*) is able to resolve structures down to ≈ 1 μm. For small slit widths, <20 μm, the measured $\Delta\lambda$ is larger than the dashed line, which is attributed to imaging aberrations of the FFG. According to the theoretical calculations of Nakano *et al.* (*9*) the present FFG images a point source into a line of width $\Delta x_{\min} = 7$ μm. The corresponding limit in wavelength resolution,

$$\Delta\lambda = \frac{d\lambda}{dx}\,\Delta x_{\min} \qquad [1]$$

is indicated in Fig. 5 by the dashed–dotted horizontal line. The wavelength resolution, $\Delta\lambda = 0.037$ Å, measured with the 5-μm slit, is close to this theoretical limit.

Thus we find as the best value of the resolving power, $\lambda/\Delta\lambda \approx 1500$ at λ between 50 and 60 Å. For larger wavelengths we could not measure the resolving power directly, because no lines were available with negligible plasma broadening. However, the best value may be calculated by the relation

$$\frac{\lambda}{\Delta\lambda} \approx \frac{r_2}{\Delta x_{\min}} \sqrt{\frac{m\lambda}{2a}}, \qquad [2]$$

where a is the grating period (=8333 Å) and m the order of diffraction. Equation [2] was obtained by using for the inverse linear dispersion an approximate formula

$$\frac{d\lambda}{dx} \approx \frac{1}{r_2} \sqrt{\frac{2a\lambda}{m}}, \qquad [3]$$

which is correct within 10% (for $\lambda \geq 50$ Å). For $\lambda = 200$ Å we find from Eq. [2] with $\Delta x_{\min} = 7$ μm a resolving power $\lambda/\Delta\lambda = 3600$. The improvement which can be obtained by using higher diffraction orders is $\propto \sqrt{m}$.

GRATING EFFICIENCY

As is evident from the measured spectra in Fig. 2 the FFG operates quite efficiently in higher diffraction orders. From such line spectra we have analyzed the grating efficiency η_m in higher diffraction orders, m, relative to the first order grating efficiency η_1 and have plotted the result in Fig. 6 as a function of the wavelength for the diffraction orders $m = 2$ to $m = 5$. In the case of the second order diffraction a few data measured by Edelstein *et al.* (*12*) with a synchrotron source have been added. Typically we find

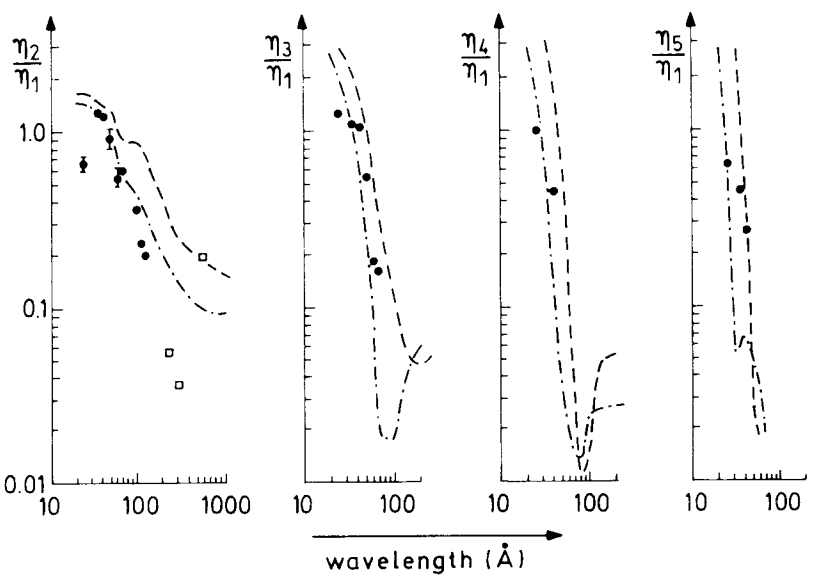

FIG. 6. Higher order grating efficiencies η_m normalized to the first order efficiency as a function of wavelength. Included are data points of Edelstein *et al.* (open squares). The dashed and the dashed-dotted curves are calculated for the blaze angles 3.2° and 2.5°, respectively.

large values of η_m/η_1 at short wavelengths of 30 to 40 Å followed by a rapid decrease with wavelength.

In addition we have determined the absolute grating efficiency of the first diffraction order. It is defined as the energy diffracted into the first order normalized to the energy incident on the FFG. For this purpose we measured (in the same laser shot) the quasicontinuous spectrum emitted by a laser irradiated gold target with the FFS and a transmission grating spectrometer (TGS) with known efficiency (*2, 13*). The first order grating efficiency of the FFG follows from

$$\eta_{\mathrm{FFG}}(\lambda) = \frac{1}{R_c} F \eta_{\mathrm{TGS}} \frac{\epsilon_{\mathrm{FFS}}(\lambda)}{\epsilon_{\mathrm{TGS}}(\lambda)}. \qquad [4]$$

The factor F contains geometrical constants and the linear dispersion of the two spectrometers. R_c denotes the reflection coefficient of the collector mirror, for which tabulated values by Henke *et al.* (*14*) for gold have been used (according to these data R_c increases from ≈ 0.6 at $\lambda = 30$ Å to ≈ 0.9 at $\lambda = 120$ Å). The quantities ϵ_{FFS} and ϵ_{TGS} are the energy densities on film recorded by the two spectrometers. Since the same type of x-ray film (Kodak 101-01) was used in both spectrometers, only the relative γ-curve (*15*) is important for the ratio $\epsilon_{\mathrm{FFS}}/\epsilon_{\mathrm{TGS}}$, and the result is not influenced by the spectral response of the film sensitivity. At wavelengths $\geqslant 90$ Å, the spectrum measured by the FFS had to be corrected for higher diffraction order contributions.

The result of this analysis is plotted in Fig. 7 (thick solid curve). We find that η_{FFG} increases rapidly with wavelength and reaches a plateau at ≈ 0.03 at larger wavelengths $\geqslant 60$ Å. The dip in efficiency at the carbon edge ($\lambda = 44$ Å) is attributed to a thin layer of carbon (probably caused by pumping oil) on the collector mirror and the FFG. Also shown in Fig. 7 are data measured by Kiehn *et al.* (*8*) and by Edelstein *et al.* (*12*) in a range of larger wavelengths. The data of these authors are by a factor ≈ 3 higher than ours. This discrepancy is attributed to an underestimation of the collector mirror reflectivity R_c, the actual value of which may be smaller than the ideal values of Ref. (*14*) due to scattering losses from the collector mirror, which has no special x-ray surface quality.

We have also calculated grating efficiencies theoretically. For this purpose we used the formulas derived by Lukirskii and Savinov (*16*) for blazed x-ray reflection gratings under grazing incidence. The required input data are the geometrical grating properties (number of grooves per length, grazing angle of incidence, and blaze angle) and the complex refractive index, which was taken from Henke *et al.* (*14*) for $\lambda \leqslant 30$ Å and from Hagemann *et al.* (*17*) for $\lambda \geqslant 30$ Å (the two data sets were smoothly joined). The formulas of Ref. (*16*) are developed for plane gratings with uniformly spaced grooves. To include the effect of the curvature and the nonuniform groove spacing of the present FFG, we calculated the efficiency for different grating surface elements and integrated it over the total grating surface to obtain the overall efficiency.

The results are plotted in Figs. 6 and 7 (the dashed and the dashed–dotted curves). Although the general trends of the measurement are reproduced quite well, no exact quantitative agreement between the calculations and the experiment could be achieved. In particular the absolute value of the first order efficiency is considerably larger in the calculation than in the experiment (Fig. 7). The discrepancies may be caused by

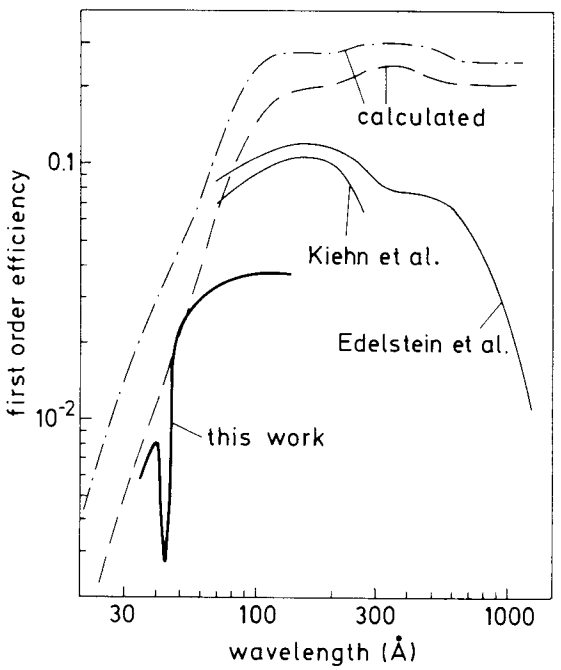

FIG. 7. First order grating efficiency as a function of wavelength. Solid curves: results measured by us and other authors; dashed and dashed–dotted curves: calculated as in Fig. 6.

differences between the refractive index taken from Refs. (*14, 17*) and its actual value. Also a critical parameter is the blaze angle, which may deviate from the value (3.2°) specified by the manufacturer. The calculations have been performed for two blaze angles, namely 3.2° (dashed curves) and 2.5° (dashed–dotted curves). The smaller angle fits somewhat better the measured relative higher order efficiencies (Fig. 6).

CONCLUSIONS

We have described a compact and practical XUV spectrometer with a commercially available flat-field grating of 1200 grooves per millimeter. Imaging of the source on a slit by a curved grazing incidence mirror makes it possible to record intense spectra even for low source energies and to optimize the spectral resolution by using narrow slits. In this way we achieve the maximum resolving power which is limited only by the imaging aberrations of the flat-field grating. It ranges from 1500 at 50 Å to 3600 at 200 Å.

We have also measured the grating efficiencies for higher orders as a function of wavelength. This data are important for analyzing spectra and unfolding them for higher order contributions.

ACKNOWLEDGMENT

This work was supported in part by the Commission of the European Communities in the framework of the Euratom-IPP Association.

REFERENCES

1. N. M. CEGLIO, R. L. KAUFMAN, A. M. HAWRILUK, AND H. MEDECKI, *Appl. Opt.* **22,** 318 (1983).
2. K. EIDMANN, T. KISHIMOTO, P. HERRMANN, J. MIZUI, R. PAKULA, R. SIGEL, AND S. WITKOWSKI, *Laser Particle Beams* **4,** 521 (1986).
3. J. A. R. SAMSON, "Techniques of Vacuum Ultraviolett Spectroscopy," Wiley, New York, 1967.
4. R. J. FONCK, A. T. RAMSEY, AND R. V. YELLE, *Appl. Opt.* **21,** 2115 (1982).
5. T. KITA, T. HARADA, N. NAKANO, AND H. KURODA, *Appl. Opt.* **22,** 512 (1983).
6. M. C. HETTRICK, J. H. UNDERWOOD, P. J. BATSON, AND M. J. ECKART, *Appl. Opt.* **27,** 200 (1988).
7. T. HARADA AND T. KITA, *Appl. Opt.* **19,** 3987 (1980).
8. G. P. KIEHN, T. GARVEY, R. A. SMITH, O. WILLI, A. R. DAMERELL, AND J. WEST, *Proc. SPIE* **831,** 150 (1988).
9. N. NAKANO, H. KURODA, T. KITA, AND T. HARADA, *Appl. Opt.* **23,** 2386 (1984).
10. G. D. TSAKIRIS, *Proc. SPIE* **1032,** 910 (1989).
11. B. L. HENKE, F. G. FUJIWARA, M. A. TESTER, C. H. DITTMORE, AND M. A. PALMER, *J. Opt. Soc. Am. B.* **1,** 828 (1984).
12. J. EDELSTEIN, M. C. HETTRICK, S. MROWKA, P. JELINSKI, AND C. MARTIN, *Appl. Opt.* **23,** 3267 (1984).
13. K. EIDMANN, M. KÜHNE, P. MÜLLER, AND G. D. TSAKIRIS, *J. X-ray Sci. Technol.* **2,** 259 (1990).
14. B. L. HENKE, P. LEE, T. J. TANAKA, R. L. SHIMABUKURO, AND B. K. FUJIKAWA, *Atomic Data Nuclear Data Tables* **27,** 1 (1982).
15. W. SCHWANDA AND K. EIDMANN, *Appl. Opt.* **31,** 554 (1992).
16. A. P. LUKIRSKII AND E. P. SAVINOV, *Opt. Spectrosc.* **14,** 147 (1963).
17. H. J. HAGEMANN, W. GUDAT, AND C. KUNZ, "Optical Constants from the Far Infrared to the X-ray Region: Mg, Al, Cu, Ag, Bi, C, and Al_2O_3," Deutsches Electronen-Synchrotron Report SR-74/7, Hamburg, 1974, unpublished.